Physics Letters B 787 (2018) 146–152

Contents lists available at ScienceDirect

Physics Letters B

www.elsevier.com/locate/physletb

On the origin of forward–backward multiplicity correlations in *pp* collisions at ultrarelativistic energies

L.V. Bravina [a,*], J. Bleibel [b,c], E.E. Zabrodin [a,d,e]

[a] Department of Physics, University of Oslo, PB 1048 Blindern, N-0316 Oslo, Norway
[b] Institut für Angewandte Physik, Universität Tübingen, Auf der Morgenstelle 10, D-72076 Tübingen, Germany
[c] Max-Planck-Institut für Intelligente Systeme, Heisenbergstr. 3, D-70569 Stuttgart, Germany
[d] Skobeltzyn Institute for Nuclear Physics, Moscow State University, RU-119899 Moscow, Russia
[e] National Research Nuclear University "MEPhI" (Moscow Engineering Physics Institute), Kashirskoe highway 31, RU-115409 Moscow, Russia

ARTICLE INFO

Article history:
Received 6 October 2016
Received in revised form 6 September 2018
Accepted 26 October 2018
Available online 30 October 2018
Editor: J.-P. Blaizot

ABSTRACT

We study multiplicity correlations of hadrons in forward and backward hemispheres in *pp* inelastic interactions at energies 200 GeV $\leq \sqrt{s} \leq$ 13 TeV within the microscopic quark–gluon string model. The model correctly describes (i) the almost linear dependence of average multiplicity in one hemisphere on the particle multiplicity in other hemisphere in the centre-of-mass frame; (ii) the increase of the slope parameter b_{corr} with rising collision energy; (iii) the quick falloff of the correlation strength with increase of the midrapidity gap; (iv) saturation of the forward–backward correlations at very high multiplicities. Investigation of the sub-processes on partonic level reveals that these features can be attributed to short-range partonic correlations within a single string and superposition of several sub-processes containing different numbers of soft and hard Pomerons with different mean multiplicities. If the number of Pomerons in the event is fixed, no forward–backward correlations are observed. Predictions are made for the top LHC energy $\sqrt{s} = 13$ TeV.

1. Introduction

The study of correlations between particles, produced in hadronic or nuclear collisions at high energies, can help us to reveal dynamical features of multiparticle production [1,2]. Among the first correlations measured in hadronic interactions, primarily (anti)proton–proton ones, were the multiplicity correlations between hadrons emitted in forward and in backward hemispheres, respectively, in the centre-of-mass frame of the reaction. These corrections were extensively studied, e.g., by the UA5 Collaboration in $\bar{p}p$ collisions at ISR energies from $\sqrt{s} = 200$ GeV to 900 GeV [3–5]. The linear dependence of the average multiplicity of particles emitted in forward hemisphere $\langle n_F \rangle$ on the particle multiplicity in backward hemisphere n_B, and vice versa, has been reported in [6]

$$\langle n_F(n_B) \rangle = a + b_{corr} n_B \,, \tag{1}$$

where

$$b_{corr} = \frac{\langle n_F n_B \rangle - \langle n_F \rangle^2}{\langle n_F^2 \rangle - \langle n_F \rangle^2} \,. \tag{2}$$

Later on the linear dependence of the forward–backward (FB) correlations was also observed in *pp* and $\bar{p}p$ collisions at lower and higher energies, varying from $p_{lab} = 32$ GeV/*c* ($\sqrt{s} = 7.86$ GeV) [7] and $p_{lab} = 250$ GeV/*c* ($\sqrt{s} = 22$ GeV) [8] to c.m. energies $0.3 \leq \sqrt{s} \leq 1.8$ TeV [9]. At Large Hadron Collider (LHC), ALICE Collaboration has confirmed the linear rise of $\langle n_B \rangle$ with increasing n_F in *pp* collisions at $\sqrt{s} = 0.9$, 2.76 and 7 TeV [10]. Note that the distribution $\langle n_F(n_B) \rangle$ deviates from linear behaviour in the range of high particle multiplicities. In e^+e^- annihilation, in contrast, only very weak FB correlations were found [11,12]. These peculiarities attract significant attention of theorists; see, e.g., [13–23] and references therein.

Nowadays, the interest to the correlation phenomena in hadronic interactions is raised because of the search for collective phenomena, such as anisotropic flow, in these collisions. In the case of heavy ion collisions, superposition of the first flow harmonics can explain the characteristic long range correlations in rapidity space colloquially known as *ridge* (see [24,25] and references therein). Similar structure was found in high multiplicity *pp* collisions as well [26]. It remains an open question still whether or not the

* Corresponding author.
E-mail address: larissa.bravina@fys.uio.no (L.V. Bravina).

https://doi.org/10.1016/j.physletb.2018.10.053

ridge in pp interactions is an initial-state or rather final-state (i.e., collective) effect. The study of the FB correlations can shed light on the origin of long range correlations emerging in hadronic collisions at ultrarelativistic energies.

Application of quark–gluon string model (QGSM) [27–31] for the description of FB correlations in pp and $\bar{p}p$ collisions at $p_{lab} = 32$ GeV/c [7] was probably the first attempt to uncover the role of different sub-processes of particle production in the formation of FB correlations within the Monte Carlo (MC) microscopic model. Subsequently, these correlations were studied in pp and $\bar{p}p$ collisions at higher energies within several microscopic models [20,32–35]. What about the quark–gluon string model? Obviously, the set of diagrams describing the variety of partonic sub-processes at hundreds and thousands GeV differs from that corresponding to ten GeV. The relative contribution of each diagram also depends on the collision energy. Therefore, our present study is focused on pp interactions in the energy range $0.9 \le \sqrt{s} \le 13$ TeV. A brief description of the basic principles of QGSM is given in Sec. 2. The forward–backward multiplicity correlations are studied in Sec. 3. In particular, we demonstrate absence of the FB correlations in each sub-class of events and appearance of strong positive correlations within the whole event sample. Obtained results are also compared with the available experimental data. Conclusions are drawn in Sec. 4.

2. Quark–gluon string model

Both the quark–gluon string model [27–29] and the dual parton model [32] are based on the $1/N$ series expansion [36,37] of the amplitude for a QCD process. This approach is also known as *topological expansion*. For high energy processes with small momentum transfer there is a one-to-one correspondence between the diagrams arising in the topological expansion and the graphs corresponding to the exchange of Regge singularities, Reggeons and Pomerons, in the Reggeon field theory (RFT) [38,39]. Thus, the QGSM obeys the requirements of unitarity and analyticity. The amplitudes of multiparticle processes are found by cutting the diagrams in the s-channel. This procedure leads to formation of new objects, quark–gluon strings, which fragment into new hadrons and resonances during the breakup stage.

The Monte Carlo version of QGSM used for present calculations has been employed for the description of hadronic, nuclear and hadron–nucleus interactions, e.g., in [7,30,31,40–43]. Although the model contains a rich set of pre-asymptotic diagrams for hadron–hadron collisions at intermediate energies, at ultrarelativistic energies its number significantly shrinks. Here the total cross section of pp interaction consists of just few terms, namely

$$\sigma_{tot}^{pp}(s) = \sigma_{el} + \sigma_P(s) + \sigma_{SD}(s) + \sigma_{DD}(s)\,, \tag{3}$$

where the terms in the rhs represent the cross sections of elastic, (multi)Pomeron, single-diffractive and double-diffractive processes, respectively. Diagrams corresponding to last three processes are shown in Fig. 1. To find the cross sections of single-diffractive and double-diffractive processes displayed in Fig. 1(c)–(g) we use the parameterization [43] of the QGSM calculations made in [44]

$$\sigma_{SD}(s) = 0.68\,\left(1 + 36\,s^{-1}\right)\,\ln\left(0.6 + 0.2\,s\right)\,, \tag{4}$$

$$\sigma_{DD}(s) = 1.65 + 0.27\,\ln s\,. \tag{5}$$

It follows from the Froissart bound $\sigma_{tot} \propto (\ln s)^2$ that the cross section of the diffractive processes should rise as $\sigma_D \propto \ln s$. Indeed, both $\sigma_{SD}(s)$ and $\sigma_{DD}(s)$ in Eqs. (4), (5) obey this asymptotic relation.

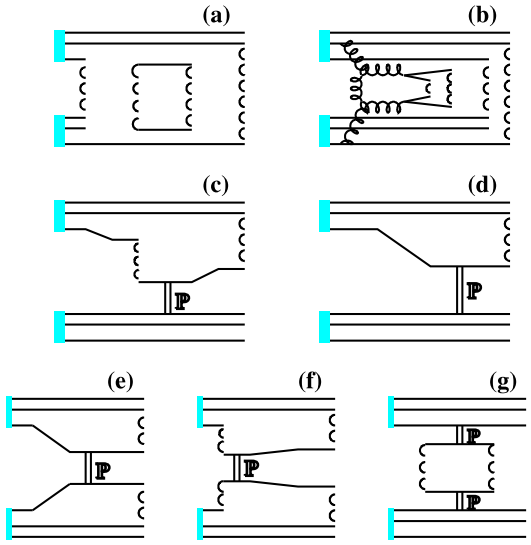

Fig. 1. Diagrams taken into account in QGSM in the modelling of pp interactions at ultrarelativistic energies: (a) multi-Pomeron exchange, (b) (semi)hard gluon–gluon interaction and soft Pomeron exchange, (c)–(d) single diffraction with high-mass and low-mass excitation, (e)–(f) double diffraction with low-mass and high-mass excitation, (g) central diffraction.

At ultrarelativistic energies, the processes going via exchange of soft Pomerons, shown in Fig. 1(a), should be completed by the hard Pomeron exchanges which lead to formation of hadronic jets, see Fig. 1(b). This feature is attributed to all RFT-based MC models designed for the description of ultrarelativistic hadron–hadron and heavy-ion collisions [32,40,45–47]. By means of the Abramovskii–Gribov–Kancheli (AGK) cutting rules [48] the inelastic nondiffractive cross section is expressed as

$$\sigma_{ND}(s) = \sum_{i,j=0;i+j\ge 1} \sigma_{ij}(s)\,, \tag{6}$$

where

$$\sigma_{ij}(s) = 2\pi \int_0^\infty bdb\,\exp\left[-2u^R(s,b)\right] \times \frac{\left[2u^R_{soft}(s,b)\right]^i}{i!}\,\frac{\left[2u^R_{hard}(s,b)\right]^j}{j!}\,. \tag{7}$$

Here b is the impact parameter, and superscript R indicates real part of the eikonal $u(s,b) = u_{soft}(s,b) + u_{hard}(s,b)$. According to [49], both soft and hard eikonals can be cast in a form

$$u^R_{s/h}(s,b) = z_{s/h}(s)\,\exp\left[-\frac{\beta^2}{4\,\lambda_{s/h}(s)}\right]\,, \tag{8}$$

$$z_{s/h}(s) = \frac{\gamma_P}{\lambda_{s/h}(s)}\,\left(\frac{s}{s_0}\right)^{\Delta}\,, \tag{9}$$

$$\lambda_{s/h}(s) = R_P^2 + \alpha'_P\,\ln\left(\frac{s}{s_0}\right)\,. \tag{10}$$

The quantities γ_P and R_P are Pomeron–nucleon vertex parameters, $\alpha_P(0)$ and α'_P are the intercept and the slope of the Pomeron trajectory, respectively, $\Delta \equiv \alpha_P - 1$, and s_0 is a scale parameter. Numerical values of the principal parameters are listed in Table 1. The relative contributions of soft and hard Pomerons to particle spectra are energy dependent. At LHC energies the number of hard Pomerons per a single pp collision significantly increases, thus

Table 1
Parameters of the soft and hard Pomerons used in the current version of the QGSM.

Parameter	Soft Pomeron	Hard Pomeron
γ_P	1.27475	0.021
R_P	2.0	2.4
$\alpha_P(0)$	1.15615	1.3217
α'_P	0.25	0

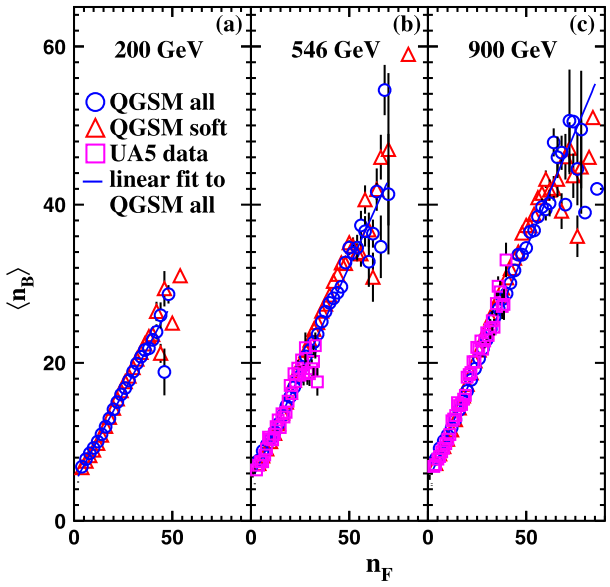

Fig. 2. Distributions $\langle n_B \rangle (n_F)$ for rapidity interval $0 \le \eta \le 4$ in NSD pp collisions at (a) $\sqrt{s} = 200$ GeV, (b) 546 GeV and (c) 900 GeV. Open triangles and circles indicate contributions of soft processes and all processes, respectively. Data from [4] are shown by open squares.

making the p_T-spectrum of secondaries harder, in full accord with the experimental data, see [43]. At very high energies one has to take into consideration Pomeron–Pomeron interactions described by the enhanced diagrams [50,51], which may cause the violation of the AGK cutting rules [52,53]. However, these diagrams are not implemented in the current version of MC QGSM.

Finally, the Field–Feynman algorithm [54] is employed to describe the fragmentation of strings with given quark content, mass and momentum into hadrons. The breakup of a string proceeds from the both edges with equal probabilities under the requirement of energy–momentum conservation and preservation of the quark content. Since no string–string interaction is taken into account, QGSM reveals only short-range correlations of hadrons in the rapidity space. Further details of the model can be found elsewhere [27–31,43].

3. Results and discussion

QGSM successfully describes FB multiplicity correlations in hadronic interactions at energies below $\sqrt{s} = 100$ GeV [7,8]. To examine the energy dependence of forward–backward correlations in pp collisions at higher energies, the interactions were generated at $\sqrt{s} = 200$, 546 and 900 GeV. For each energy ca. one million non-single diffractive events were selected. Average multiplicities of charged hadrons emitted in backward hemisphere as function of charged particle yield in forward hemisphere in non-single diffractive (NSD) pp collisions are displayed in Fig. 2 together with the available experimental results of UA5 [4] collaboration. Recall, that the cross section of $\bar{p}p$ annihilation process drops quickly with rising collision energy, thus making possible comparison of pp calculations with the $\bar{p}p$ data. To clarify the role of hard processes, Fig. 2 shows separately the FB correlations extracted from the model calculations with and without the hard Pomeron exchanges. The full distributions are fitted also to linear dependence given by Eq. (1).

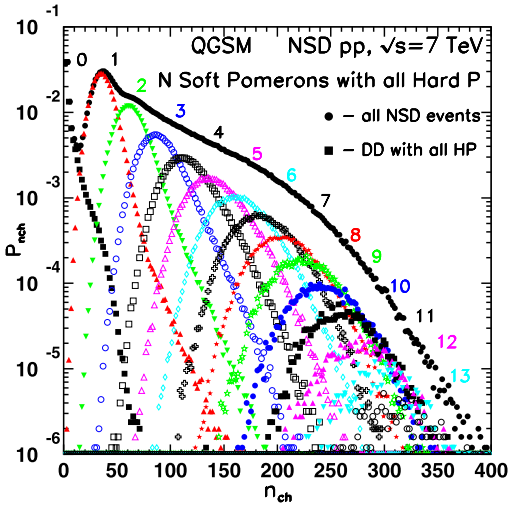

Fig. 3. Multiplicity distributions of charged hadrons in NSD pp collisions at $\sqrt{s} = 7$ TeV. Full circles and full squares denote all events and double-diffractive events together with all hard Pomerons, respectively. Other distributions are for the processes with 1, 2, etc. soft Pomerons and all hard Pomerons.

It is worth mentioning several features. (i) The shapes of the $\langle n_B \rangle (n_F)$ distributions are almost linear, except for very high n_F multiplicities. (ii) The slope parameter b_{corr} increases with rising $\sqrt{s}$ from 0.46 ± 0.01 at $\sqrt{s} = 200$ GeV to 0.59 ± 0.02 at $\sqrt{s} = 900$ GeV. (iii) QGSM calculations agree well with the UA5 data at 546 GeV and 900 GeV. (iv) There is no significant difference in FB multiplicity correlations between the model calculations with and without the hard processes, i.e. the forward–backward correlations arise mainly due to the soft processes. But, as was mentioned in Sec. 2, the model possesses only the short-range correlations due to the dynamics of string break-up. We have to scrutinize, therefore, the FB correlations arising in the sub-processes of multiparticle production in QGSM.

3.1. Forward–backward multiplicity correlations in different sub-processes

Here $4 \cdot 10^6$ pp interactions at $\sqrt{s} = 7$ TeV are considered in order to compare then the model calculations with the extensive data obtained at this energy by ALICE collaboration [10]. The multiplicity distributions of charged particles $P_{n_{ch}}(n_{ch})$ for NSD events with $i = 1, 2, \ldots, 11$ soft Pomerons are shown in Fig. 3. These distributions have a Gaussian-like structure and become broader with the increase of the number of soft Pomerons N_{s_Pom} in the event. The average multiplicity of charged hadrons also increases with rising N_{s_Pom}. Note, that sub-processes with hard Pomerons are included in the analysis.

To examine the role of hard processes, Figs. 4(a) and 4(b) depict $P_{n_{ch}}(n_{ch})$ distributions for the events with zero and with one soft Pomeron, respectively, and up to seven hard Pomerons. In events without the soft Pomerons, the hard Pomerons enhance the multiplicity distribution of double-diffractive process by ca. 50%, see Fig. 4(a). The width of the final distribution, however, is almost insensitive to the number of hard Pomerons, N_{h_Pom}. In contrast, events with one soft and several hard Pomerons, shown in Fig. 4(b), demonstrate a shift in the positions of maxima of multiplicity distributions from 40 for 1SP + 1HP events to 100 for

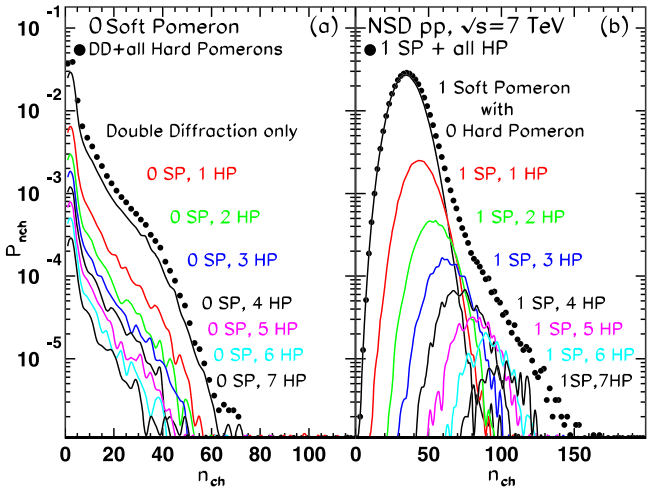

Fig. 4. Multiplicity distributions of charged hadrons in NSD pp collisions at $\sqrt{s} =$ 7 TeV for processes with (a) zero and (b) one soft Pomerons. Solid circles show the total distributions, whereas lines indicate partial contributions of sub-events with 0, 1, 2, etc. hard Pomerons.

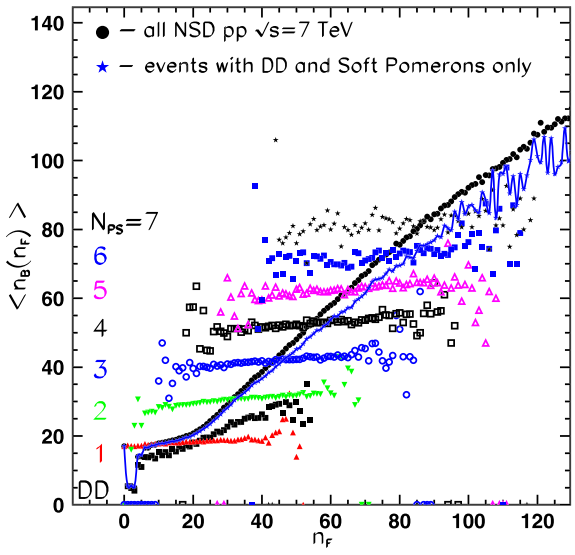

Fig. 5. Dependence of average multiplicity $\langle n_B \rangle$ on n_F in NSD pp collisions at $\sqrt{s} = 7$ TeV in QGSM. Solid circles and solid line denote the distributions for all NSD events and for the events without hard processes, respectively. Other symbols indicate $\langle n_B(n_F) \rangle$ distributions for sub-events with only soft Pomerons, $N_{s\_Pom} =$ $0, 1, \ldots, 7$.

1SP + 7HP ones. Similar effect takes place in events with two and more soft Pomerons. It causes the rise of high-multiplicity tails of the distributions shown in Fig. 3.

Fig. 5 displays dependence $\langle n_B \rangle$ on n_F for sub-events in NSD pp collisions at $\sqrt{s} = 7$ TeV without hard Pomerons and with fixed number of soft Pomerons, increasing from zero to seven. All but double-diffractive distributions are remarkably flat indicating no forward–backward multiplicity correlations within each class of selected events. However, the integrated samples of NSD collisions with and without the hard processes demonstrate clearly the positive dependence of $\langle n_B \rangle$ on n_F. Positive slope of full $\langle n_B \rangle(n_F)$ distribution confirms the statement that mixing of events with different mean values will lead to the correlations in the whole sample [32,34]. Compared to lower energies, hard processes are more abundant at LHC, and their contribution makes the slope of $\langle n_B(n_F) \rangle$ steeper. The non-zero slope of $\langle n_B(n_F) \rangle$ for double-

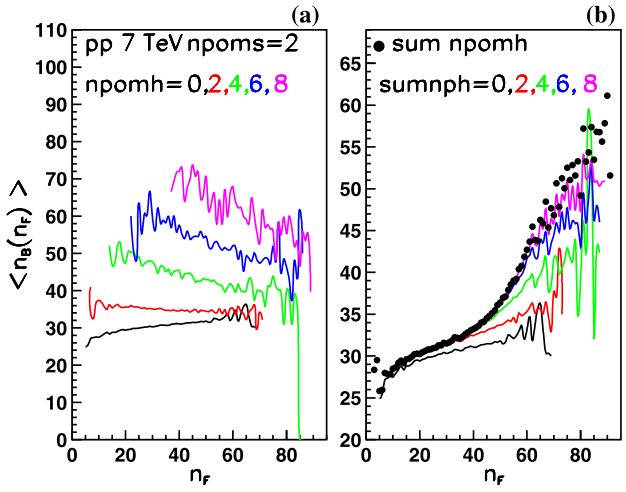

Fig. 6. The same as Fig. 5 but for sub-events with two soft Pomerons and with $N_{h\_Pom} = 0, 2, \ldots, 8$ hard Pomerons. Solid symbols show the $\langle n_B(n_F) \rangle$ dependence for all sub-events with two soft Pomerons and all hard Pomerons.

diffractive processes is also explained by mixing of sub-processes with different mean multiplicities, see Fig. 1(e)–(g).

For the events with both soft and hard Pomerons the picture is more peculiar. Dependencies $\langle n_B(n_F) \rangle$ for sub-events with two soft Pomerons and even number of hard Pomerons are shown in Fig. 6(a), whereas Fig. 6(b) depicts the combination of spectra with 2, 4, etc. hard Pomerons, presented in Fig. 6(a). With the increase of number of hard Pomerons in a sub-event, the individual distributions start to develop slightly negative slopes. But mixing up these sub-events leads to appearance of positive correlation clearly seen in Fig. 6(b). Therefore, the slope b_{corr} increases in the model with rising collision energy because more sub-processes with different mean multiplicities become available.

Recall, that the FB correlations are usually explained by the interplay of the short range correlations arising from the decay of individual sources and the long range correlations originating from the fluctuations in the number of sources. Our findings strongly support this conclusion. By selecting certain sub-events, we fix the number of strings, i.e., sources of particles. Fluctuations in the number of sources means mixing of sub-events with different amount of strings which also have different mean multiplicities.

As was shown in [20], inclusion of string–string interactions in the model via the string fusion mechanism reduces the number of strings which leads to decrease of the correlation strength b_{corr}. However, the reduction of the b_{corr} in pp interactions even at ultrarelativistic energies appears to be less than 5% because of not very high densities of the strings, in stark contrast to heavy ion collisions [20].

3.2. Comparison with the experimental data

Average values of $\langle n_B(n_F) \rangle$ in NSD pp collisions at $\sqrt{s} = 7$ TeV reported in [10] were obtained under the kinematic cuts $0.3 \leq p_T \leq 1.5$ GeV/c and $0 \leq \eta \leq 0.8$. Model calculations shown in Fig. 7 agree reasonably well with the data. The average multiplicities $\langle n_B \rangle$ and accessible multiplicity intervals in n_F for the processes with $n = 1, \ldots, 7$ soft Pomerons indicate that all subprocesses contribute to events with charged particle multiplicity n_F below 10, while for higher n_F the number of contributed topologies is reduced. As a consequence, the slope of $\langle n_B(n_F) \rangle$ becomes more acclivous. Note, however, that the imposed kinematic cuts completely remove the contributions from double-diffractive processes in addition to the single-diffractive ones. To show this

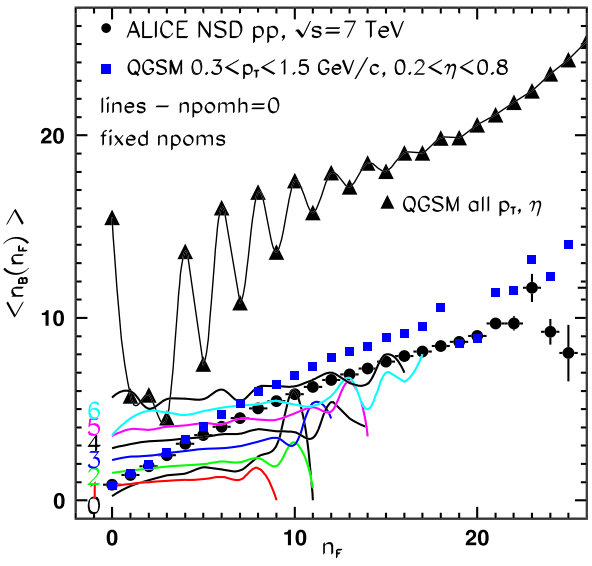

Fig. 7. The same as Fig. 5 but for hadrons within the kinematic region $0.3 \leq p_T \leq 1.5$ GeV/c and $0.2 \leq \eta \leq 0.8$. Solid squares and circles indicate QGSM calculations and ALICE data from [10], respectively. Solid triangles denote the calculations of NSD events in full phase space.

we plot in Fig. 7 QGSM calculations for NSD pp events in full range of rapidity and transverse momentum. One can see characteristic oscillations of $\langle n_B(n_F)\rangle$ distribution at $n_F \leq 16$, arising in diffractive events because of the charge conservation. Namely, the mid-rapidity gap is large and the most typical configurations are odd numbers of charged particles in each hemisphere. For even number of charged hadrons in forward hemisphere there should be emission of one particle from backward hemisphere. The process is likely to occur in high-multiplicity diffraction after the decays of resonances. The odd multiplicities in low n_F region do not need this constraint. Therefore, for low number of n_F the oscillations in FB correlations are quite significant, whereas the larger the number n_F, the less pronounced the peaks are.

Further analysis is done in terms of midrapidity gaps η_{gap}, hadrons of which are excluded from the investigation, and the widths of selected pseudorapidity bins $\delta\eta$ in both hemispheres. Following [10], we vary the η_{gap} from 0 to 1.2 and perform the study for $\delta\eta = 0.2, 0.4, 0.6$ and 0.8. These distributions are displayed in Fig. 8 for NSD pp collisions at $\sqrt{s} = 900$ GeV, 2.76 TeV, 7 TeV and 13 TeV. Comparing the model results with the data obtained at first three energies, one can see that QGSM both quantitatively and qualitatively describes two general features. Firstly, parameter b_{corr} increases with broadening of $\delta\eta$ at fixed rapidity gap η_{gap}. Secondly, for fixed $\delta\eta$ the strength of FB multiplicity correlations drops with increasing midrapidity gap η_{gap} in accord with the observations at lower energies [4,7]. This means that the string processes contribute to FB correlations in central rapidity region, whereas for well-separated areas in forward and backward hemispheres the long-range FB correlations are absent. Predictions made for correlations at $\sqrt{s} = 13$ TeV show further increase of b_{corr}. The decrease of the slope parameter at fixed $\delta\eta$ with rising η_{gap} is not so steep because of the broadening of midrapidity region.

The FB multiplicity correlations are studied in different azimuthal sectors for pp collisions at 900 GeV and 7 TeV. The model calculations are plotted onto the ALICE data in Fig. 9. The width of the rapidity bin is $\delta\eta = 0.2$ and the azimuthal angle of each sector is $\varphi = \pi/4$. Similar to analysis shown in Fig. 8, the midrapidity gap varies from $\eta_{gap} = 0.2$ to 1.4. Note, that the results at 7 TeV are reduced by factor 2. Except of the absolute strength of

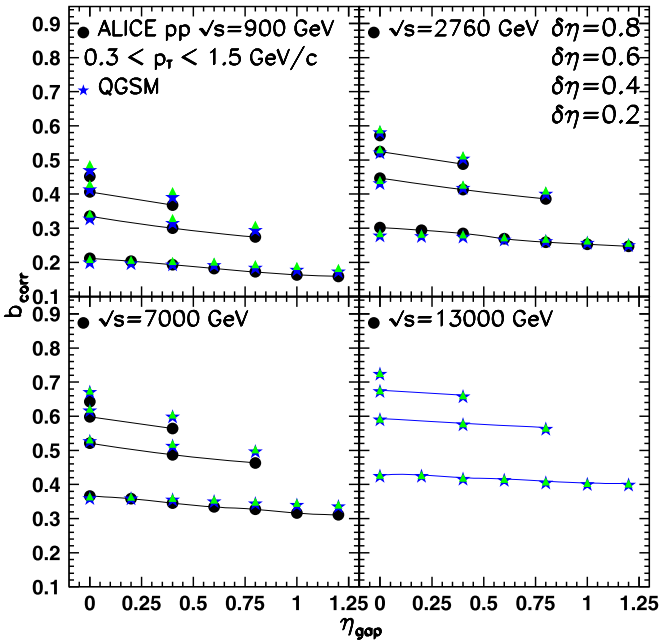

Fig. 8. FB correlation parameter b_{corr} as a function of η_{gap} in four rapidity bins (from bottom to top): $\delta\eta = 0.2, 0.4, 0.6, 0.8$ in pp collisions at $\sqrt{s} = 900$ GeV, 2.76 TeV, 7 TeV and 13 TeV. Stars and circles denote the model calculations and the ALICE data from [10], respectively. Lines are drawn to guide the eye.

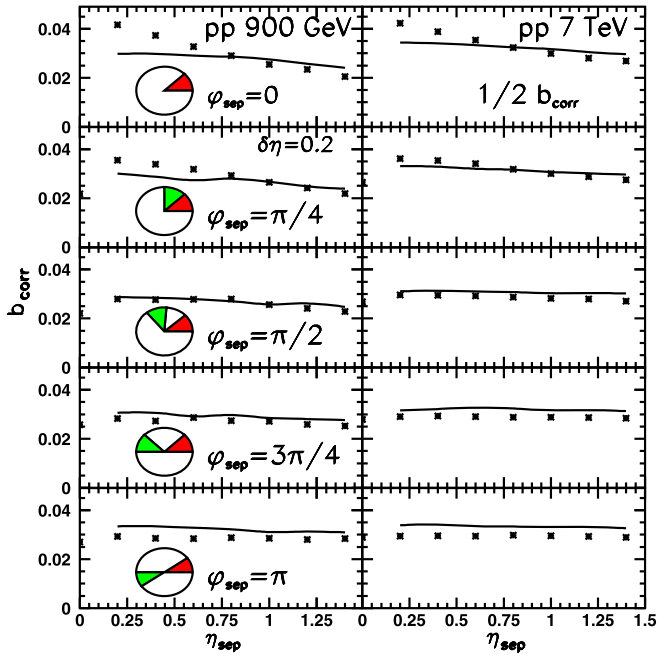

Fig. 9. FB correlation parameter b_{corr} for azimuthally separated sectors of $\varphi = \pi/4$ as a function of midrapidity gap at fixed $\delta\eta = 0.2$ in pp collisions at $\sqrt{s} = 900$ GeV (left column) and 7 TeV (right column). Results for 7 TeV are reduced by factor 2. Lines and asterisks denote the model calculations and the data from [10], respectively.

the correlations, there is a very weak difference between the distributions at 900 GeV and 7 TeV. The correlation strength between the different sectors in Fig. 9 is order of magnitude weaker compared to azimuthally integrated results shown in Fig. 8. It is worth noting the different φ-dependence of the FB correlations at midrapidity and in more peripheral regions. At $\eta_{gap} = 0.2$ the strength of the correlations drops slightly with φ_{sep} rising from zero to π,

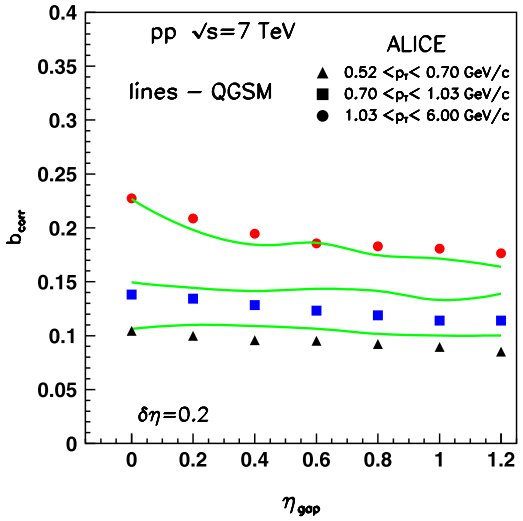

Fig. 10. FB correlation parameter b_{corr} for windows of width $\delta\eta = 0.2$ as a function of η_{gap} in three p_T intervals: 0.52 GeV/$c \le p_T <$ 0.70 GeV/c (bottom curve), 0.70 GeV/$c \le p_T <$ 1.03 GeV/c (medium curve), and 1.03 GeV/$c \le p_T <$ 6.0 GeV/c (upper curve) in QGSM calculations of pp collisions at $\sqrt{s} = 7$ TeV. Symbols denote the data from [10].

whereas at $\eta_{gap} = 1.2$ a weak increase of the b_{corr} is observed. QGSM reproduces the correlations in $\eta - \varphi$ windows at both energies quite well. The 20% underestimation of the near-side rise of the correlation strength at small $\Delta\eta$ can be attributed to relative lack of resonances in the model.

Finally, Fig. 10 displays the correlation parameter b_{corr} for windows of width $\delta\eta = 0.2$ as a function of η_{gap} in different transverse momentum intervals in pp collisions at $\sqrt{s} = 7$ TeV. Data obtained by ALICE Collaboration [10] are plotted onto the QGSM calculations as well. We see that b_{corr} increases for hadrons with larger p_T for all intervals η_{gap}. These data help us to discriminate between the possible scenarios of jet distribution in pseudorapidity. If the jets are uniformly distributed, the p_T dependence of the b_{corr} in QGSM is similar to that obtained in PHOJET model (see Fig. 13b of [10]). Correct description of the data, shown in Fig. 10, is attained if one assumes the Gaussian distribution of jets in η-space.

4. Conclusions

Multiplicity correlations in forward and backward hemispheres are studied in pp collisions at energies 200 GeV $\le \sqrt{s} \le$ 13 TeV within the quark–gluon string model. No tuning of the free parameters of the model was performed. The linear dependence of $\langle n_B \rangle$ on n_F is reproduced within the whole energy range. The main contribution to the FB correlations comes from the multistring processes due to multi-Pomeron exchanges. These processes have different multiplicity distributions, and the FB multiplicity correlations arise because of superposition of such sub-processes with different mean multiplicities. For the events with fixed amount of soft and hard Pomerons the forward–backward correlations are absent. The increase of the variety of sub-processes explains the rise of the correlation strength b_{corr} with increasing collision energy. Deviation of the $\langle n_B(n_F) \rangle$ distributions from linear behaviour in the range of high n_F multiplicities is due to reduction of number of multi-particle processes contributing to these events.

Comparison with experimental data shows that QGSM correctly reproduces (i) increase of b_{corr} with rising $\sqrt{s}$; (ii) increase of b_{corr} with broadening width of the bin $\delta\eta$ at midrapidity range; (iii) decrease of b_{corr} with increasing (mid)rapidity gap $\Delta\eta$ between the tested FB particle samples; and (iv) FB multiplicity correlations in $\eta - \varphi$ windows. Experimental data on changing of $b_{corr}(\eta_{gap})$ with rising transverse momentum favour the Gaussian distribution of jets in pseudorapidity. Predictions are made for $\sqrt{s} = 13$ TeV. Also, we predict oscillations in strength of FB correlations in both single-diffractive and double-diffractive collisions in the full phase space. In these interactions the distributions $\langle n_B(n_F) \rangle$ should peak at even values of n_F and drop at odd n_F values for $n_F \le 16$. The origin of the oscillations is linked to the conservation of electric charge.

Acknowledgements

The authors are grateful to I. Altsybeev for consultations concerning the analysis of ALICE data. This work was supported by the Norwegian Research Council (NFR) under grant No. 255253/F50 – CERN Heavy Ion Theory. J.B. thanks the German Research Foundation (DFG) for the financial support through the Project BL 1286/2-1. L.B. acknowledges financial support of the Alexander von Humboldt Foundation.

References

[1] E.A. De Wolf, I.M. Dremin, W. Kittel, Phys. Rep. 270 (1996) 1.
[2] V. Koch, in: R. Stock (Ed.), Relativistic Heavy Ion Physics, in: Landolt–Börnstein Database, vol. 23, Springer, Berlin, 2010, pp. 626–652.
[3] K. Alpgaard, et al., UA5 Collab., Phys. Lett. B 123 (1983) 361.
[4] G.G. Alner, et al., UA5 Collab., Phys. Rep. 154 (1987) 247.
[5] R.E. Ansorge, et al., UA5 Collab., Z. Phys. C 37 (1988) 191.
[6] S. Uhlig, I. Derado, R. Meinke, H. Preissner, Nucl. Phys. B 132 (1978) 15.
[7] L.V. Bravina, et al., Sov. J. Nucl. Phys. 50 (1989) 245.
[8] V.V. Aivazyan, et al., NA22 Collab., Z. Phys. C 42 (1989) 533.
[9] T. Alexopoulos, et al., E735 Collab., Phys. Lett. B 353 (1995) 155.
[10] J. Adam, et al., ALICE Collab., J. High Energy Phys. 05 (2015) 097.
[11] W. Braunschweig, et al., TASSO Collab., Z. Phys. C 45 (1989) 193.
[12] R. Akers, et al., OPAL Collab., Phys. Lett. B 320 (1994) 417.
[13] A. Capella, A. Krzywicki, Phys. Rev. D 18 (1978) 4120.
[14] A. Capella, J. Tran Thanh Van, Z. Phys. C 18 (1983) 85.
[15] J. Dias de Deus, Phys. Lett. B 100 (1981) 177.
[16] T.T. Chou, C.N. Yang, Phys. Lett. B 135 (1984) 175.
[17] B. Carazza, Nuovo Cimento 99 (1988) 731.
[18] S. Barshay, Phys. Lett. B 199 (1987) 121.
[19] L.K. Chen, D. Kiang, C.K. Chew, Phys. Lett. B 408 (1997) 422.
[20] N.S. Amelin, et al., Phys. Rev. Lett. 73 (1994) 2813.
[21] N. Armesto, M.A. Braun, E.G. Ferreiro, C. Pajares, Nucl. Phys. A 661 (1999) 325c.
[22] M.A. Braun, C. Pajares, V.V. Vechernin, Phys. Lett. B 493 (2000) 54.
[23] V.V. Vechernin, Nucl. Phys. A 939 (2015) 21.
[24] K. Aamodt, et al., ALICE Collaboration, Phys. Rev. Lett. 107 (2011) 032301.
[25] G. Aad, et al., ATLAS Collaboration, Phys. Rev. C 86 (2012) 014907.
[26] V. Khachatryan, et al., CMS Collaboration, J. High Energy Phys. 1009 (2010) 091.
[27] A.B. Kaidalov, Phys. Lett. B 116 (1982) 459.
[28] A.B. Kaidalov, K.A. Ter-Martirosyan, Phys. Lett. B 117 (1982) 247.
[29] A.B. Kaidalov, Phys. Usp. 46 (2003) 1121.
[30] N.S. Amelin, L.V. Bravina, Sov. J. Nucl. Phys. 51 (1990) 133.
[31] N.S. Amelin, L.V. Bravina, L.I. Sarycheva, L.N. Smirnova, Sov. J. Nucl. Phys. 51 (1990) 535.
[32] A. Capella, U. Sukhatme, C.I. Tan, J. Tran Thanh Van, Phys. Rep. 236 (1994) 225.
[33] Y.-L. Yan, et al., Nucl. Phys. A 834 (2010) 320c.
[34] K. Wraight, P. Skands, Eur. Phys. J. C 71 (2011) 1628.
[35] V. Kovalenko, V. Vechernin, DESY Conf. Proc. 2014-04/82 (2014) 691, arXiv: 1410.3884 [hep-ph].
[36] G. t'Hooft, Nucl. Phys. B 75 (1974) 461.
[37] G. Veneziano, Phys. Lett. B 52 (1974) 220.
[38] V. Gribov, Sov. Phys. JETP 26 (1968) 414.
[39] L.V. Gribov, E.M. Levin, M.G. Ryskin, Phys. Rep. 100 (1983) 1.
[40] N.S. Amelin, E.F. Staubo, L.P. Csernai, Phys. Rev. D 46 (1992) 4873.
[41] L.V. Bravina, et al., Phys. Rev. C 60 (1999) 044905.
[42] E.E. Zabrodin, C. Fuchs, L.V. Bravina, Amand Faessler, Phys. Lett. B 508 (2001) 184.
[43] J. Bleibel, L.V. Bravina, E.E. Zabrodin, Phys. Rev. D 93 (2016) 114012.
[44] A.B. Kaidalov, M.G. Poghosyan, Eur. Phys. J. C 67 (2010) 397.
[45] K. Werner, F.-M. Liu, T. Pierog, Phys. Rev. C 74 (2006) 044902.
[46] R. Engel, J. Ranft, S. Roesler, Phys. Rev. D 52 (1995) 1459.
[47] S. Ostapchenko, Nucl. Phys., Proc. Suppl. 151 (2006) 143; S. Ostapchenko, Phys. Rev. D 83 (2011) 014018.
[48] V. Abramovskii, V. Gribov, O. Kancheli, Sov. J. Nucl. Phys. 18 (1974) 308.

[49] A. Capella, J. Tran Thanh Van, J. Kweicinski, Phys. Rev. Lett. 58 (1987) 2015.
[50] O.V. Kancheli, JETP Lett. 11 (1970) 267.
[51] A.H. Mueller, Phys. Rev. D 2 (1970) 2963.
[52] Y.V. Kovchegov, K. Tuchin, Phys. Rev. D 65 (2002) 074026.
[53] E. Levin, A. Prygarin, Phys. Rev. C 78 (2008) 065202.
[54] R.D. Field, R.P. Feynman, Nucl. Phys. B 136 (1978) 1.